Ultrafast Exciton Dynamics in a ZnO Thin Film

Hsiang-Chen Wang*, C. C. Yang[1], Shih-Wei Feng[2], Bao-Ping Zhang[3], and Yusaburo Segawa[3]

Graduate Institute of Opto-Mechatronics, National Chung Cheng University, Chia-Yi, Taiwan, R.O.C.
[1]*Graduate Institute of Electro-Optical Engineering and Department of Electrical Engineering, National Taiwan University, Taipei, Taiwan, R.O.C.*
[2]*Department of Applied Physics, National University of Kaohsiung, Kaohsiung, Taiwan, R.O.C.*
[3]*Photodynamics Research Center, RIKEN (The Institute of Physical and Chemical Research), Sendai 980-0845, Japan*

Received July 14, 2008; accepted November 15, 2008; published online February 20, 2009

We report the behavior of utrafast exciton dynamics in a ZnO thin film based on temperature-, pump-energy-, and pump-power-dependent degenerate pump–probe experiments. When the pump energy is higher than the emission peak, either dominated by free exciton or donor-bound exciton, a Stokes shift of about 20 meV can be observed. In this situation, rapid thermalization process (in several ps) followed by an exciton relaxation stage (7 to 104 ps) is recorded. The relaxation into the donor-bound exciton level takes a longer time because a spatial transport process is required. When the pump energy is lower than the emission peak, the optical-field-induced red shift of the absorption spectrum results in an enhanced absorption for the probe can be observed. This effect recovers in several ps.

DOI: 10.1143/JJAP.48.022402

1. Introduction

Exciton recombination for effective photon emission at room temperature (due to a large bulk exciton binding energy at 60 meV) in ZnO has made this semiconductor attractive for the development of light-emitting devices. The exciton binding strength can be even stronger when a ZnO/MgZnO quantum well structure is formed.[1)] The generation of the P-line of a stimulated emission under intense excitation further implies efficient emission through exciton-exciton scattering.[2,3)] In addition to free exciton (FX) recombination, the emission of biexcitons (XX) has also been observed at low temperatures.[4,5)] Because of the larger XX binding energy in a quantum well structure, emission of XX at room temperature becomes possible. Since the recombination rate of XX is higher than that of FX, XX emission at room temperature can lead to even higher radiation efficiency in a light-emitting device based on ZnO. In the past several years, significant progress in ZnO crystal quality has been achieved. In addition to nano-structures such as nano-tubes,[6,7)] nano-rods,[8,9)] and nano-walls,[10)] high-quality ZnO thin films have been grown by molecular beam epitaxy,[11,12)] metal–organic chemical vapor-phase deposition,[13–15)] pulsed-laser deposition,[16,17)] and sputtering.[18,19)]

Although the basic optical properties of exciton systems in various semiconductors have been widely studied,[20–22)] those of ZnO deserve more investigation because high-quality ZnO epi-crystals were not available until recently.[13,23)] In particular, because of the existence of abundant intrinsic donors of shallow nature in ZnO, FX and donor-bound excitons (D^0X) are normally mixed in the spectral distribution.[22,24,25)] Hence, the study of the photon emission processes, including ultrafast exciton dynamics,[5,22,26,27)] of ZnO require more efforts. In this paper, we report the results and interpretation of the fs pump–probe experiment on a high-quality ZnO thin film. By varying the sample temperature and pump photon energy, the exciton relaxation processes related to the Stokes shift and the optical-field-induced red shift were observed. The relaxation time constants as functions of various variables are calibrated. The optical-field-induced red shift of the absorption spectrum results in an enhanced absorption for the probe. This effect is recovered in several ps.

In this paper, the sample structure and experimental setup are explained in §2. Here, the basic photoluminescence properties of the sample are also described. Then, the results of the pump–probe spectroscopy are presented in §3. These results are interpreted and discussed in §4. Finally, the conclusions are drawn in §5.

2. Experimental Procedure

The ZnO thin film was grown by metal–organic chemical vapor deposition on (0001) sapphire substrate at a pressure of 6 Torr at 450 °C for 90 min. The growth pressure and temperature were chosen based on the optimized conditions for growing high-quality ZnO thin films on sapphire.[28)] In the growth of ZnO, oxygen gas and diethyl zinc [$Zn(C_2H_5)_2$, DEZn] were used as precursors, and nitrogen was used as the carrier gas for the DEZn. For both samples, the O_2 flow was 30 sccm, the N_2 flow was 5 sccm, and the temperature of DEZn was 4 °C. The thickness of the thin film is about 1 μm. This sample has been studied by scanning electron microscopy (SEM) and high-resolution transmission electron microscopy (HRTEM). The SEM images showed a surface morphology of spiral domain structures. The HRTEM images showed high-quality crystalline structures in the sample except for certain threading dislocations along the *c*-axis within a domain.[29,30)] The basal plane of ZnO is twisted by 30° from that of sapphire to minimize the strain energy. The backside of the sapphire substrate was polished for transmission measurements.

The second-harmonic of a 76-MHz, 100-fs mode-locked Ti:sapphire laser with a BBO crystal was used for the degenerate pump–probe experiment. The cut angles of the BBO crystal were $\theta = 32.96°$. The thickness of the crystal was $d = 0.4$ mm. The second-harmonic tuning range was 3.349 to 3.442 eV. Over the entire tuning range, the full-width at half-maximum (FWHM) of the second-harmonic pulse was about 150 fs. The corresponding spectral FWHM was about 10 nm. The pump beam was defocused onto a spot 150 μm in diameter, which was about two times the probe beam size, to ensure the uniform pump illumination of the probe region.

*E-mail address: hcwang@ccu.edu.tw

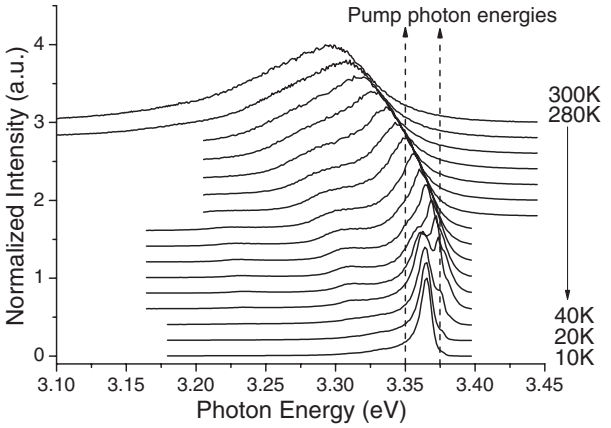

Fig. 1. Temperature-dependent PL spectra. The two dashed lines indicate the photon energies (3.349 and 3.375 eV) of the degenerate pump and probe, respectively.

Figure 1 shows the temperature-dependent photoluminescence (PL) spectra. At 10 K, FX (at 3.376 eV) and D^0X (at 3.365 eV) are separated by about 11 meV. Below 60 K, D^0X dominates the emission. Above 80 K, FX intensity becomes stronger. At room temperature, the dominating FX emission leads to a broad spectrum, which mixes with the emission features of a donor–acceptor pair and a one-phonon-assisted transition. The two dashed lines indicate the photon energies of the degenerate pump and probe. The higher energy at 3.375 eV roughly corresponds to the FX level at low temperatures. The lower energy at 3.349 eV is below the PL spectral peak when the temperature is lower than 180 K.

3. Results

Figure 2 shows the temperature-dependent, time-resolved differential transmission ($\Delta T/T$) traces from the pump–probe experiment with the pump–probe energy at 3.349 eV. The pump and probe powers are 8 and 0.8 mW, respectively. To obtain the exciton decay/recovery times, we used an impulse response function to fit the measured data:

$$u(t)[a_0\delta(t) + a_1 e^{-t/\tau_1} + a_2 e^{-t/\tau_2}], \qquad (1)$$

where $u(t)$ is the unit step function, $\delta(t)$ is the impulse associated with the two-photon instantaneous decrease at time zero with a negative amplitude a_0, $a_1 e^{-t/\tau_1}$ is a fast decay component with a time constant τ_1 of about 150 fs, and τ_2 is about 20 ps. Fitting results illustrated by the red dashed curves in Fig. 2. From previous studies of ZnO nanorods,[31–34] the slow component $a_2 e^{-t/\tau_2}$ is attributed to the relaxation of the band filling effect, dominated by nonradiative carrier recombinations. It is interesting to note the sign change of this a_2 component below 30 K when the pump beam photon energy is about 3.349 eV (see Fig. 2), due to the depression of the ac Stark effect. Through carrier recombination, the exciton thermalization and the depression of the ac Stark effect are recovered. At 180 K, at which temperature the pump photon energy coincides with the PL spectral peak, the sample material responds weakly to the pump. In other words, under these conditions, the ZnO does not significantly absorb photons. Below this temperature, the time-resolved probe intensity profile first shows a peak, corresponding to the exciton filling effect due to the pump

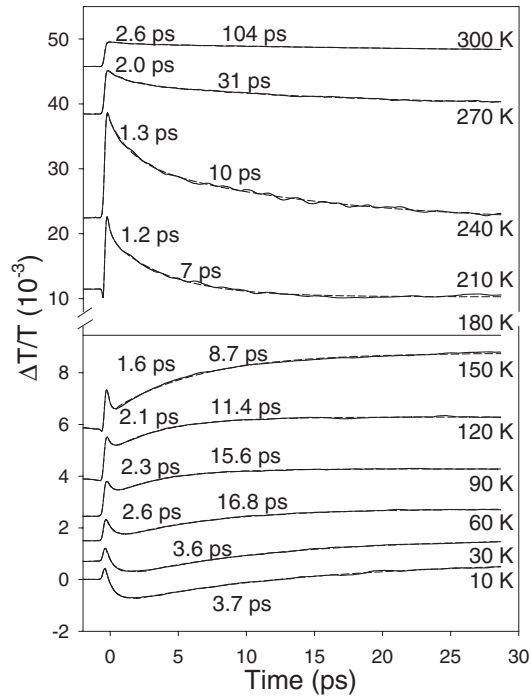

Fig. 2. Temperature-dependent, time-resolved differential transmission traces with the pump–probe energy at 3.349 eV. Red dashed curves are convolutions of fits.

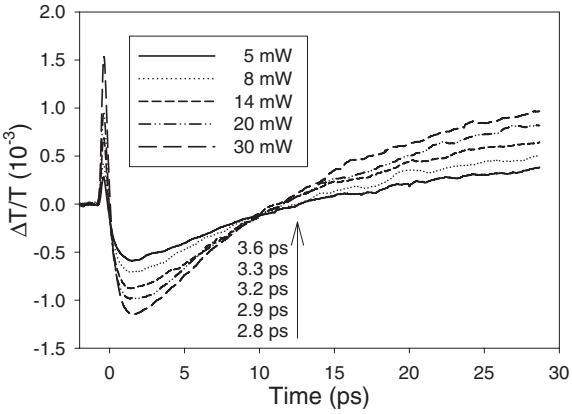

Fig. 3. Pump-power-dependent differential transmission traces for a pump–probe energy of 3.349 eV at 10 K.

overlap, and then a depression, followed by an increase. The minimum of the depression is lower than the zero-pump level when the temperature is lower than 60 K. Between 60 and 180 K, a two-component increase after the minimum is observed. On the other hand, beyond 180 K, each pump–probe trace shows a peak, followed by a two-component decay. The decay-time constants become longer as temperature increases. The decay-time constants are given next to the decay curves.

Figure 3 shows the pump-power-dependent differential transmission traces for a pump–probe energy of 3.349 eV at 10 K. The probe power was maintained at 0.8 mW. One can see that the minimum level decreases with pump power, implying that higher pump intensity leads to stronger absorption and faster recovery of the probe. Figure 4 shows the pump–probe-energy-dependent (3.349, 3.375, 3.394, 3.418, and 3.442 eV) differential transmission traces at

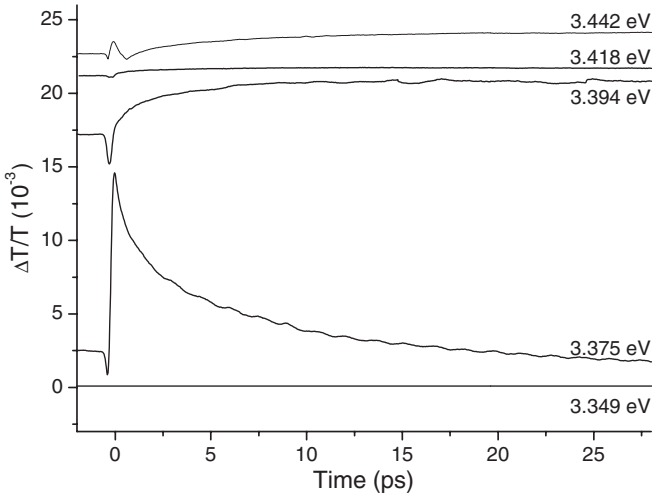

Fig. 4. Pump–probe-energy-dependent differential transmission traces at 180 K.

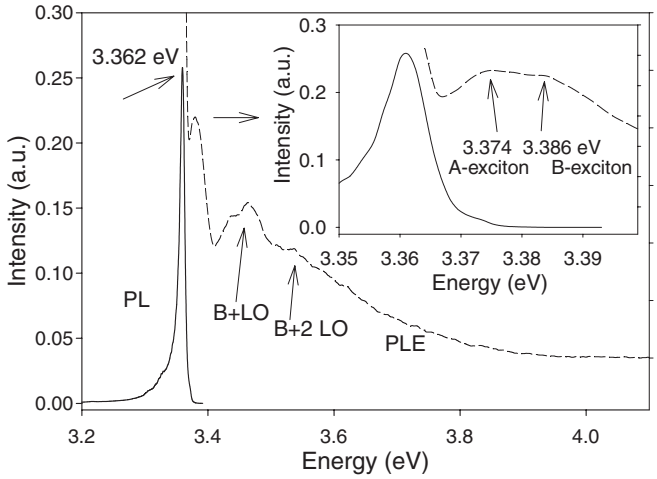

Fig. 6. PL (continuous curve) and PLE (dashed curve) spectra of the sample at 10 K. The insert shows the expansion between 3.35 and 3.4 eV.

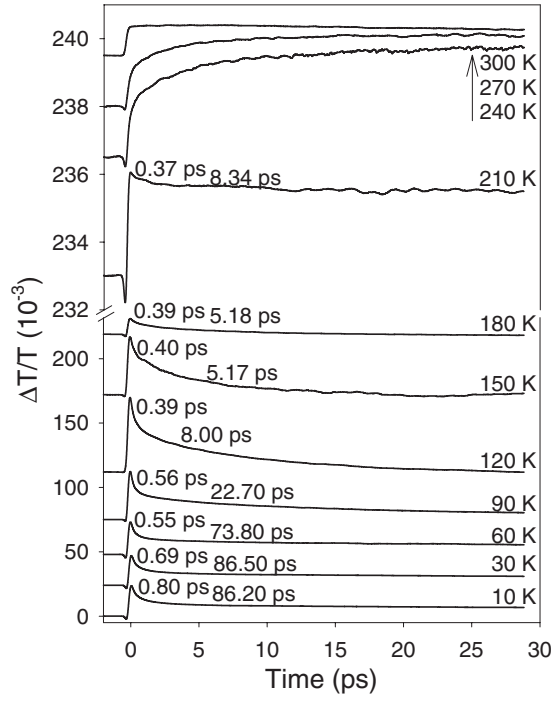

Fig. 5. Temperature-dependent differential transmission traces for a pump–probe energy of 3.375 eV.

180 K. The pump and probe powers are fixed at 8 and 0.8 mW, respectively. The zero-response at 3.349 eV is again seen. When the pump photon energy increases by 26 meV, a strong variation in pump–probe differential transmission is observed. The fast rise followed by a sharp decay is similar to the curve at 240 K in Fig. 2. As the pump photon energy increases to 3.394 eV, the rise becomes smooth. The narrow dips at 3.375 and 3.394 eV correspond to two-photon absorption of the sample. As the pump energy is further increased, the sample response becomes weaker. At 3.442 eV, the pump–probe behavior is similar to that of those below 60 K in Fig. 2.

Figure 5 shows the temperature-dependent differential transmission traces for a pump–probe energy of 3.375 eV. Here, one can see similar trace patterns with a rise followed by a two-component decay up to 210 K. At 240 and 270 K, a slow increase in the pump–probe trace is observed. The response of the sample to the pump at this photon energy diminishes as room temperature is approached. It is interesting to note that no significant fast transient corresponding to the exciton thermailization process is evident when the exciton density is below the Mott density,[35] which is quite different from previous studies of other semiconductors such as GaN,[36] GaAs,[37] and InGaAs.[38] When the photoexcited exciton density was above the Mott density, excitons were ionized into electron–hole plasmas and an extra fast time constant of about 0.3–0.8 ps appeared. For the data shown in Fig. 5, we used a higher pump photon energy, about 3.375 eV, than for that shown in Fig. 2. In such a high photon energy, the exciton density is above the Mott density, and the electron–hole plasmas can be generated.

4. Discussion

To interpret the pump–probe behavior, the photoluminescence excitation (PLE) spectrum at 10 K was measured, as shown in Fig. 6. Here, the PLE and PL spectra are depicted by dashed and continuous curves, respectively. The insert shows the expansion between 3.35 and 3.4 eV. In the PLE spectrum, one can see several absorption peaks, corresponding to different types of excitons (excitons A and B) and phonon-assisted features.[39] In Fig. 6, a Stokes shift of about 20 meV is observed.[39] Such a Stokes shift usually represents the energy difference between the maximum state population and the low-energy tail. This Stokes shift can be used to explain the pump–probe behavior above 180 K in Fig. 2. Here, the maximum response to the pump occurs near 240 K, at which point the PL peak is lower than the pump energy by about 23 meV (see Fig. 1). In other words, at 240 K the absorption maximum roughly coincides with the pump energy. Because the FX emission dominates above 180 K, the decays in the curves in Fig. 2 in this temperature range correspond to the relaxation of carriers into the emission levels of FX. The first-stage decay describes the thermalization process (within a couple of ps) of excitons toward a quasi-equilibrium condition. The decay time of the first

component slightly increases with temperature owing to the hot phonon effect.[40] The excitons reabsorb energy from hot phonons, and such a process dominates when phonon density increases with temperature. In addition, the second-stage decay results from the relaxation process of excitons into FX emission levels. As the absorption energy level moves further away from the emission level, the relaxation becomes slower (from 7 to 104 ps). At higher temperatures beyond 180 K, excitons have more excess energy due to larger energy differences between the band gap energy and the pump photon energy in Fig. 1. When excitons have more excess energy, exciton–exciton scattering and exciton–phonon scattering dominate in the relaxation process. This slows down the exciton relaxation process. On the other hand, phonon-assisted relaxation is apparent when the pump photon energy is much larger than the band gap energy. At second-stage decay, these two events slow down the exciton relaxation process above 180 K. The almost zero-response at 180 K in Fig. 2 can be attributed to the almost zero absorption when the pump energy coincides with the emission peak. In Fig. 4, the strong response to the pump at 3.375 eV also shows a Stokes shift of about 20 meV. The smooth increase after the two-photon-absorption-induced dip at 3.394 eV may be due to the relaxation of excitons into the probe energy state from the two-photon level or other higher energy states.

The patterns of the pump–probe trace below 210 K in Fig. 5 are similar to those beyond 180 K in Fig. 2. In Fig. 5, the maximum response occurs between 120 and 150 K. Here, a Stokes shift of about 20 meV is again observed. In this situation above 90 K, carriers relax into the FX emission levels after rapid thermalization (0.4 ps in the time scale). The relaxation time constants are comparable to their counterparts in Fig. 2. However, below 90 K, the exciton relaxation becomes slower (several tens ps in the time scale). This trend can be attributed to the required transport process for excitons to be trapped by D^0X since D^0X dominates the emission in this temperature range.

The pump–probe behavior below 180 K when the pump energy is 3.349 eV is quite different from that discussed above. The depressions after the peaks are attributed to the ac Stark effect.[41,42] In this process, once a strong optical field is applied to a semiconductor around the absorption edge, a red shift of the absorption spectrum is induced. Hence, an absorption increase can be observed, as shown in the pump–probe traces at 10 and 30 K in Fig. 2. As temperature increases, the pump energy becomes closer to the emission peak owing to the thermally induced red shift. In this situation, the effect of the ac Stark process becomes weaker and hence the depression minima in the temperature range between 60 and 150 K become higher than the zero-pump level. The rapid first recovery stage (1.6 to 3.7 ps for the recovery time constant) represents an important feature of the ac Stark effect.[41,42] The slower second recovery stage corresponds to the exciton relaxation process. In Fig. 3, the depression minimum becomes lower as the pump power increases because the ac Stark effect is stronger under stronger pumping. With stronger pumping, the recovery from the absorption spectrum red shift becomes faster, as confirmed by the decreasing recovery time with increasing pump power.

5. Conclusions

In conclusion, we have discussed the ultrafast exciton dynamic behavior in a ZnO thin film based on temperature-, pump-energy-, and pump-power-dependent degenerate pump–probe experiments. When the pump energy was higher than the emission peak, either dominated by FX or D^0X, a Stokes shift of about 20 meV was observed. In this situation, a fast thermalization process (in a couple of ps) followed by an exciton relaxation stage (several to tens ps) was recorded. The relaxation into the D^0X level took a longer time because a spatial transport process was required. When the pump energy was lower than the emission peak, the optical-field-induced red shift was observed in the absorption spectrum. This effect recovered in several ps.

Acknowledgment

This research was supported by the National Science Council, The Republic of China, under grant NSC 97-2218-E-194-001.

1) C. H. Chia, T. Makino, K. Tamura, and Y. Segawa: Appl. Phys. Lett. **82** (2003) 1848.
2) D. Magde and H. Mahr: Phys. Rev. Lett. **24** (1970) 890.
3) A. Ohtomo, K. Tamura, M. Kawasaki, T. Makino, Y. Segawa, Z. K. Tang, G. K. L. Wong, Y. Matsumoto, and H. Koinuma: Appl. Phys. Lett. **77** (2000) 2204.
4) H. J. Ko, Y. F. Chen, and T. Yao: Appl. Phys. Lett. **77** (2000) 537.
5) F. Y. Jen, Y. C. Lu, C. Y. Chen, H. C. Wang, C. C. Yang, B. P. Zhang, and Y. Segawa: Appl. Phys. Lett. **87** (2005) 072103.
6) X. W. Sun, S. F. Yu, C. X. Xu, C. Yuen, B. J. Chen, and S. Li: Jpn. J. Appl. Phys. **42** (2003) 229.
7) B. P. Zhang, N. T. Binh, K. Wakatsuki, Y. Segawa, Y. Yamada, N. Usami, M. Kawasaki, and H. Koinuma: Appl. Phys. Lett. **84** (2004) 4098.
8) W. I. Park, Y. H. Jun, S. W. Jung, and G. Yi: Appl. Phys. Lett. **82** (2003) 964.
9) X. Liu, X. Wu, H. Cao, and R. P. H. Chang: J. Appl. Phys. **95** (2004) 3141.
10) H. T. Ng, J. Li, M. K. Smith, P. Nguyen, A. Cassell, J. Han, and M. Meyyappan: Science **300** (2003) 1249.
11) Y. Chen, D. Bagnall, and T. Yao: Mater. Sci. Eng. B **75** (2000) 190.
12) D. C. Look, D. C. Reynolds, C. W. Litton, R. L. Jones, D. B. Eason, and G. Cantwell: Appl. Phys. Lett. **81** (2002) 1830.
13) K. Haga, T. Suzuki, Y. Kashiwaba, H. Watanabe, B. P. Zhang, and Y. Segawa: Thin Solid Films **433** (2003) 131.
14) Th. Gruber, C. Kirchner, K. Thonke, R. Sauer, and A. Waag: Phys. Status Solidi A **192** (2002) 166.
15) B. P. Zhang, K. Wakatsuki, N. T. Binh, N. Usami, and Y. Segawa: Thin Solid Films **449** (2004) 12.
16) H. L. Porter, A. L. Cai, J. F. Muth, and J. Narayan: Appl. Phys. Lett. **86** (2005) 211918.
17) F. K. Shan, G. X. Liu, W. J. Lee, G. H. Lee, I. S. Kim, and B. C. Shin: Appl. Phys. Lett. **86** (2005) 221910.
18) S. F. Chichibu, T. Yoshida, T. Onuma, and H. Nakanishi: J. Appl. Phys. **91** (2002) 874.
19) D. K. Hwang, H. S. Kim, J. H. Lim, J. Y. Oh, J. H. Yang, S. J. Park, K. K. Kim, D. C. Look, and Y. S. Park: Appl. Phys. Lett. **86** (2005) 151917.
20) T. Amand, B. Dareys, B. Baylac, X. Marie, J. Barrau, M. Brousseau, D. J. Dunstan, and R. Planel: Phys. Rev. B **50** (1994) 11624.
21) S. Nüsse, P. H. Bolivar, H. Kurz, V. Klimov, and F. Lery: Phys. Rev. B **56** (1997) 4578.
22) F. Y. Jen, Y. C. Lu, C. Y. Chen, H. C. Wang, C. C. Yang, B. P. Zhang, and Y. Segawa: Appl. Phys. Lett. **87** (2005) 252117.
23) K. Hazu, T. Sota, K. Suzuki, S. Adachi, S. F. Chichibu, G. Cantwell, D. B. Eason, D. C. Reynolds, and C. W. Litton: Phys. Rev. B **68**

(2003) 033205.
24) S. B. Zhang, S.-H. Wei, and A. Zunger: Phys. Rev. B **63** (2001) 075205.
25) D. C. Reynolds, D. C. Look, B. Jogai, C. W. Litton, T. C. Collins, W. Harsch, and G. Cantwell: Phys. Rev. B **57** (1998) 12151.
26) T. Tokizaki, H. Sakai, A. Nakamura, Y. Manabe, S. Hayashi, and T. Mitsuyu: Semicond. Sci. Technol. **10** (1995) 1253.
27) A. Yamamoto, T. Kido, T. Goto, Y. Chen, T. Yao, and A. Kasuya: Appl. Phys. Lett. **75** (1999) 469.
28) B. P. Zhang, N. T. Binh, K. Wakatsuki, Y. Segawa, Y. Yamada, N. Usami, M. Kawasaki, and H. Koinuma: J. Phys. Chem. B **108** (2004) 10899.
29) C. Y. Chi, S. C. Chin, Y. C. Lu, L. Hong, Y. L. Lin, F. Y. Jen, C. C. Yang, B. P. Zhang, and Y. Segawa: Nanotechnology **16** (2005) 3084.
30) W. Y. Shiao, C. Y. Chi, S. C. Chin, C. F. Huang, T. Y. Tang, Y. C. Lu, Y. L. Lin, L. Hong, F. Y. Jen, C. C. Yang, B. P. Zhang, and Y. Segawa: J. Appl. Phys. **99** (2006) 054301.
31) J. Collet and T. Amand: Phys. Rev. B **33** (1986) 4129.
32) D. C. Reynolds, D. C. Look, B. Jogai, J. E. Hoelscher, R. E. Sherriff, N. T. Harris, and M. J. Callahan: J. Appl. Phys. **88** (2000) 2152.
33) S. Hong, T. Joo, W. I. Park, Y. H. Jun, and G.-C. Yi: Appl. Phys. Lett. **83** (2003) 4157.
34) J. C. Johnson, K. P. Knutsen, H. Yan, M. Law, Y. Zhang, P. Yang, and R. J. Saykally: Nano Lett. **4** (2004) 197.
35) N. Peyghambarian, S. W. Koch, and A. Mysyrowicz: *Introduction to Semiconductor Optics* (Prentice Hall, Upper Saddle River, NJ, 1993) Chap. 13.
36) C.-K. Sun, Y.-C. Huang, G.-W. Chern, K.-H. Lin, and J.-C. Liang: Appl. Phys. Lett. **81** (2002) 85.
37) W. H. Knox, R. L. Fork, M. C. Downer, D. A. B. Miller, D. S. Chemla, C. V. Shank, A. C. Gossard, and W. Wiegmann: Phys. Rev. Lett. **54** (1985) 1306.
38) M. Wegener, I. Bar-Joseph, G. Sucha, M. N. Slam, N. Sauer, T. Y. Chang, and D. S. Chemla: Phys. Rev. B **39** (1989) 12794.
39) T. Makino, Y. Segawa, M. Kawasaki, and H. Koinuma: Semicond. Sci. Technol. **20** (2005) S78.
40) C.-K. Sun, F. Vallee, S. Keller, J. E. Bowers, and S. P. Denbaars: Appl. Phys. Lett. **70** (1997) 2004.
41) A. Mysyrowicz, D. Hulin, A. Antonetti, A. Migus, W. T. Masselink, and H. Morkoc: Phys. Rev. Lett. **56** (1986) 2748.
42) W. H. Know, D. S. Chemla, D. A. B. Miller, J. B. Stark, and S. Schmitt-Rink: Phys. Rev. Lett. **62** (1989) 1189.